J Mol Model
DOI 10.1007/s00894-010-0726-4

ORIGINAL PAPER

The binding modes and binding affinities of artemisinin derivatives with *Plasmodium falciparum* Ca^{2+}-ATPase (PfATP6)

Pradeep Kumar Naik · Mani Srivastava · Prasad Bajaj · Sankalp Jain · Abhishek Dubey · Piyush Ranjan · Rishay Kumar · Harvinder Singh

Received: 22 January 2010 / Accepted: 19 April 2010

Abstract Noncompetitive inhibitors of sarco/endoplasmic reticulum Ca^{2+}-ATPase (SERCA) orthologue (PfATP6) of *P. falciparum* have important therapeutic value in the treatment of malaria. Artemisinin and its analogues are one such class of inhibitors which bind to a hydrophobic pocket located in the transmembrane region of PfATP6 near the biomembrane surface and interfere with calcium transport. The 3D structure of PfATP6 was modeled by homology modeling. A library consisting of 150 artemisinin analogues has been designed. Their molecular interactions and binding affinities with modeled PfATP6 protein have been studied using the docking, molecular mechanics based on generalized Born/surface area (MM-GBSA) solvation model and multi-ligand bimolecular association with energetics (eMBrAcE). Structure activity relationship models were developed between the antimalarial activity (log RA) and molecular descriptors like docking score and binding free energy. For both the cases the r^2 was in the range of 0.538–0.688 indicating good data fit and r^2_{cv} was in the range of 0.525–0.679 indicating that the predictive capabilities of the models were acceptable. Besides, a scheme similar to linear response was used to develop free energy of binding (FEB) relationship based on electrostatic (ΔG_{ele}), van der Waal (ΔG_{vdW}) and surface accessible surface area (SASA), which can express the activity of these artemisinin derivatives. It has been seen that ΔG_{vdW} has most significant correlation to the activity (log RA) and electrostatic energy (ΔG_{ele}) has less significant correlation. It indicates that the binding of these artemisinin derivatives to PfATP6 is almost hydrophobic. Low levels of root mean square error for the majority of inhibitors establish the docking, Prime/MM-GBSA and eMBrAcE based prediction model is an efficient tool for generating more potent and specific inhibitors of PfATP6 by testing rationally designed lead compound based on artemisinin derivatization.

Keywords Artemisinin · Docking · eMBrAcE · Prime MM-GBSA · Sarco/endoplasmic reticulum

P. K. Naik (✉) · M. Srivastava · P. Bajaj · S. Jain · A. Dubey · P. Ranjan · R. Kumar · H. Singh
Department of Biotechnology and Bioinformatics,
Jaypee University of Information Technology,
Waknaghat,
Solan 173215, Himachal Pradesh, India
e-mail: pknaik73@rediffmail.com

Introduction

In the 1970s, Chinese scientists identified artemisinin (*quinghaosu*) from sweet wormwood (*Artemisia annua*), thereby giving us our most important class of antimalarial drugs. The use of artemisinin contained therapies has increased exponentially [1] but the mechanism of action of these sesquiterpene lactone endoperoxides is controversial [2]. Some [3, 4], but not all [5–7], studies suggest that the mechanism of action of artemisinin is by heme-dependent activation of an endoperoxide bridge occurring within the parasite's food vacuole. However, localization of artemisinin to parasite and not food vacuole membranes [8], and killing of tiny rings lacking haemozoin argue against the food vacuole being a major site for drug action [9].

An alternative hypothesis for the mode of action of artemisinin has been proposed, based on structural similarities between the sesquiterpene moieties of thapsigargin and artemisinin (Fig. 1). Artemisinin shows structural similar-

Published online: 12 May 2010

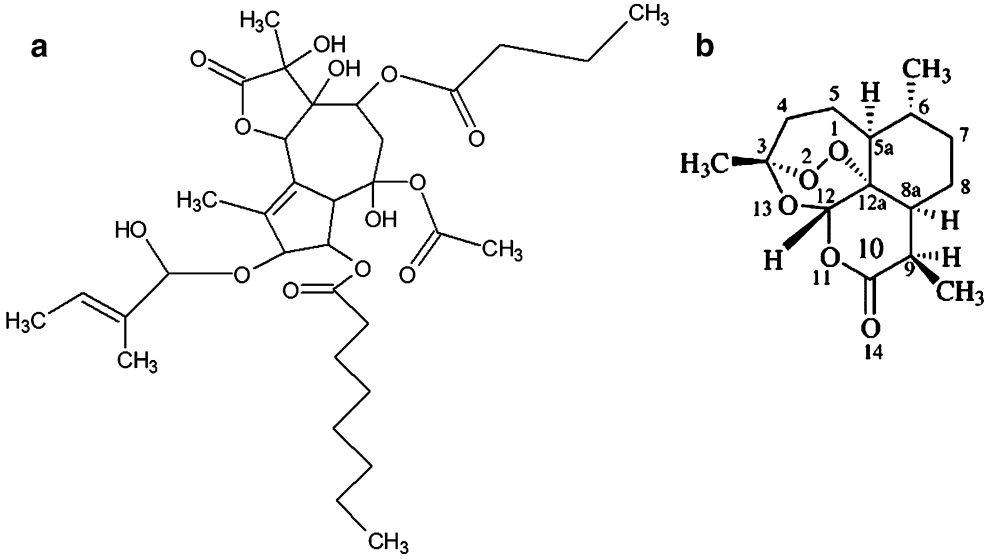

Fig. 1 The 2D structure of (**a**) Thapsigargin (TG) and (**b**) Artemisinin showing the similarity between sesquiterpene moieties

ities to thapsigargin (another plant product from *Thapsia garganica*), which is a highly specific inhibitor of sarco/endoplasmic reticulum Ca^{2+}-ATPase (SERCA). Thus it was suggested that artemisinin may act in a similar way, but specifically to inhibit the SERCA of malarial parasite. PfATP6 is the only SERCA-type Ca^{2+}-ATPase sequence in the parasite's genome and is thought to be the real molecular target of artemisinin in spite of some disagreements to be resolved [8]. The experimental studies also revealed that artemisinin inhibit the SERCA-type Ca^{2+}-ATPase orthologue (PfATP6) of *P. falciparum* in Xenopus oocytes [10].

The SERCA belongs to the family of P-type ATPases that are responsible for active transport of cations across biomembranes [11]. The SERCA uses the energy released from hydrolysis of ATP to ADP for transporting calcium ions to the lumen of sarco- and endoplasmic reticulum (ER) against the electrochemical gradient. The publications of crystal structure of nucleotide free SERCA in calcium-bound form [12] (E1.2Ca^{2+}) and in TG-bound form [13] (E2'.TG) as well as in complex form with a nonhydrolyzable ATP analogue (E1.AMPPCP) [14, 15] and in ADP stabilized by aluminum fluoride (E1.AIFx.ADP) [15] has elucidated the structures of key intermediates involved in the calcium transport cycle. The availability of such structural data has facilitated the understanding of conformational changes and dynamics involved at various steps of the transport cycle. The overall structure of SERCA consists of three cytoplasmic domains and 10 transmembrane helices. The two calcium binding sites in the E1 state of SERCA are about 5 Å apart and situated in the *trans*-membrane region, around 4 Å and 7 Å below the cytoplasmic surface of the membrane. The TG binding site is located in a hydrophobic cavity formed by transmembrane helices M3, M5, and M7. The polar end of the TG molecule is located near the membrane interface between residues Phe256 and Ile829. Binding of TG to SERCA is mostly hydrophobic in nature with only one hydrogen bond formed between Ile829 backbone and the carboxyl oxygen at O-8 position of the TG molecule. The availability of structural information on SERCA facilitates the understanding of structure-activity relationships (SAR) for SERCA inhibition and enables molecular modeling techniques to be applied for designing novel and more potent inhibitors.

The amino acid sequence of PfATP6 is known [16] but the three-dimensional structure is not available. In this study, therefore, we have constructed the 3D structure of PfATP6 by homology modeling and thereafter taken for interaction study between artemisinin and PfATP6. The utmost importance in a structure-based drug design is the reliable filtering of putative hits in terms of their predicted binding affinity (scoring problem) which is based on the in silico-generated near native protein-ligand configurations (docking problem). Most of the scoring functions used in docking programs are designed to predict binding affinity by evaluating the interaction between a compound and a receptor. However, it should be noted that ligand receptor recognition process is determined not only by enthalpic effects but also by entropic effects. Moreover, the scoring functions have a simplified form for the energy function to facilitate high throughput evaluation of a large number of compounds in a single docking run. These functions may be problematic when used with contemporary docking programs and can result in a decrease of virtual screening accuracy. To overcome this problem more precise but time consuming computational methodologies are necessary. In this study we have used several receptor-centric computational methodologies for computational modeling of artemisinin and its derivatives as potent inhibitors of PfATP6.

Fig. 2 Alignment of PfATP6 sequence with 1IWO as reference protein

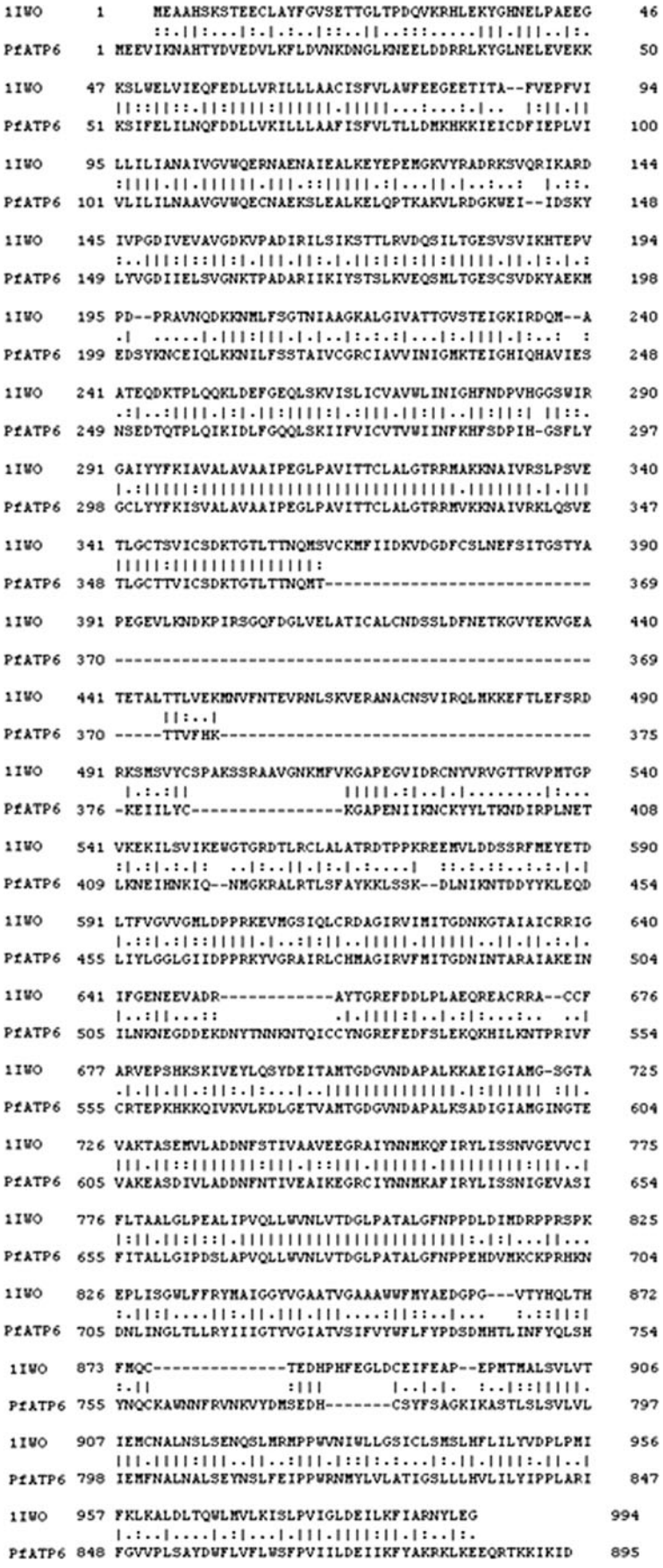

Computational methods

Sequence analysis

The protein sequence of PfATP6 of the organism *Plasmodium falciparum* was obtained from the PlasmoDB, the official database of the malaria parasite genome project [12, 13]. Gene PFA0310c located in *P. falciparum* chromosome 1 and annotated by Sanger encoded the only SERCA-type calcium transporting ATPase protein. This protein comprises 1228 amino acids. The amino acid sequence was downloaded from the web site [14]. Sequence similarity search with BLAST in Protein Data Bank (PDB) database gives only one similar protein (43.5% identical), SERCA (pdb ID: 1IWO). This structure is determined at 1.3 Å resolution and contains highly specific inhibitor thapsigargin (TG) [10]. It has three functional domains, the α-helix ion channel domain where TG is located. The binding of TG to the ion channel domain is derived almost only through hydrophobic interaction with proposed hydrogen bonding of TG O8 and 1819 backbone amide hydrogen. We performed the pairwise alignment of PfATP6 with 1IWO as reference using the homology module of PRIME [17]. We initially built the structure of PfATP6 using 1IWO as template. The structure of the PfATP6 α-helix domain is very similar to the corresponding TG-binding site of SERCA. But the ATP-binding domain and calcium ion binding domain showed relatively low similarity to SERCA. Therefore, we removed the mismatched sequence part (375–707) from the whole sequence and then constructed the three-dimensional structure of PfATP6. The sequence alignment after removing the part of mismatched sequence is shown in Fig. 2.

Table 1 Artemisinin analogues with anti-malarial activities against the drug resistant malarial strain *P. falciparum* (W-2 clone) used in this work

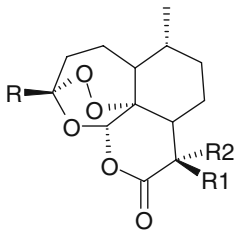

Sl No.	R	R1	R2	Log RA	pIC50 (ng/ml)
1	CH_3	CH_3	H	1.000	1.398
2	C_4H_8Ph	H	H	0.450	0.712
3	CH_3	H	2-Z-Butenyl	-1.10	-0.760
4	CH_3	H	H	0.790	1.188
5	CH_3	H	2-E-Butenyl	-0.600	-0.260
6	CH_3	Allyl	H	-0.100	0.260
7	CH_3	C_4H_9	H	0.170	0.508
8	C_4H_8Ph	C_4H_9	H	-0.320	-0.117
9	C_3H_6(P-Cl-Ph)	C_4H_9	H	-0.280	-0.097
10	$CH_2CH_2CO_2Et$	C_4H_9	H	1.360	1.595
11	CH_3	C_2H_5	H	1.400	1.777
12	CH_3	C_6H_{13}	H	0.860	1.162
13	CH_3	i- C_4H_9	H	-0.550	-0.212
14	CH_3	i-C_6H_{13}	H	-0.040	0.262
15	CH_3	i-C_3H_7	H	-0.040	0.317
16	CH_3	i-C_5H_{11}		0.070	0.389
17	$CH_2CH_2CO_2Et$	H	H	0.370	0.669
18	C_2H_5	H	H	0.050	0.448
19	C_3H_7	H	H	0.830	1.207
20	CH_3	C_3H_6(p-Cl-Ph)	H	1.370	1.595
21	CH_3	CH_2CH_3	R_1=R_2	-0.360	-0.022
22	CH_3	C_5H_{11}	H	1.020	1.339
23	CH_3	C_4H_8Ph	H	0.630	0.876
24	CH_3	C_2H_4Ph	H	0.120	0.398
25	CH_3	C_3H_6Ph	H	0.780	1.042

Table 2 10-Substituted artemisinin derivatives with anti-malarial activities against the drug resistant malarial strain *P. falciparum* (W-2 clone) used in this work

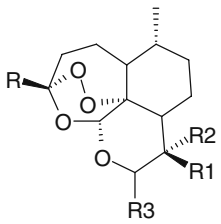

Sl. No.	R	R1	R2	R3	Log RA	pIC_{50} (ng/ml)
26	CH_3	CH_3	H	H	0.750	1.170
27	CH_3	CH_3	H	OH	0.550	0.945
28	CH_3	CH_3	H	OEt	0.340	0.694
29	CH_3	CH_3	H	OH	0.960	1.295
30	CH_3	CH_3	H	OEt	-1.080	-0.740
31	CH_3	H	Br	H	0.280	0.606
32	CH_3	CH_3	Br	NH-2-(1,3-thiazole)	0.660	0.874
33	CH_3	CH_3	Br	aniline	0.180	0.401
34	CH_3	Br	CH_3	NH-2-pyridine	-0.090	0.115
35	CH_3	CH_3	Br	NH-2-pyridine	-0.770	-0.564
36	CH_3	CH_3	H	OMe	0.280	0.654
37	CH_3	CH_3	H	α-OEt	0.320	0.674
38	CH_3	C_4H_9	H	H	1.320	1.677
39	CH_3	C_2H_5	H	H	0.670	1.068
40	CH_3	C_3H_7	H	OEt	-0.040	0.277
41	CH_3	C_2H_5	H	OEt	0.500	0.835
42	CH_3	CH_3	H	C_3H_6OH	0.780	1.115
43	CH_3	CH_3	H	OCH_2CO_2Et	0.520	0.800
44	CH_3	CH_3	H	$OC_2H_4CO_2Me$	0.100	0.364
45	CH_3	CH_3	H	$OC_3H_6CO_2Me$	-0.030	0.218
46	CH_3	CH_3	H	OCH_2(4-PhCO_2Me)	-0.070	0.143
47	CH_3	CH_3	H	(R)-$OCH_2CH(CH_3)CO_2Me$	1.790	2.070
48	CH_3	CH_3	H	(S)-$OCH_2CH(CH_3)CO_2Me$	2.250	2.530
49	CH_3	CH_3	H	(R)-$OCH(CH_3)CH_2CO_2Me$	0.870	1.134
50	CH_3	CH_3	H	(S)-$OCH(CH_3)CH_2CO_2Me$	1.700	1.964
51	$CH_2CH_2CO_2Et$	H	H	H	0.700	1.017
52	C_3H_6(p-Cl-Ph)	H	H	H	-0.550	-0.295
53	C_4H_9	H	H	H	0.750	1.127
54	C_2H_5	H	H	H	-1.000	-0.580
55	i-C_4H_9	H	H	H	0.400	0.777
56	C_3H_7	H	H	H	0.840	1.238
57	C_4H_8Ph	H	H	H	0.580	0.858
58	CH_3	-CH_2O-		OOH	-0.570	-0.219
59	CH_3	=CH_2		OOH	-0.990	-0.616
60	-	CH_3	OH	α-OH	-0.890	-0.519
61	CH_3	C_5H_{11}	H	H	0.160	0.498
62	CH_3	C_3H_6Ph	H	H	1.400	1.678
63	CH_3	C_3H_7	H	H	0.740	1.117
64	-	CH_3	OH	CH_2CF_3	0.330	0.615
65	-	OH	CH_3	CH_2CF_3	-0.700	-0.415
66	-	CH_3	OH	OEt	-0.440	-0.415
67	CH_3	CH_3	H	OOt-C_4H_9	0.920	1.217

Table 3 Seco-artemisinin derivatives with anti-malarial activities against the drug resistant malarial strain *P. falciparum* (W-2 clone) used in this work

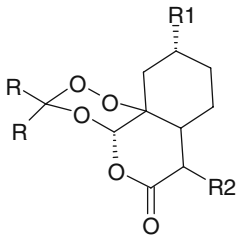

Sl. No.	R	R1	R2	Log RA	pIC_{50} (ng/ml)
68	CH_3	H	H	-2.370	-1.906
69	C_2H_5	H	H	-1.130	-0.713
70	-	-	-	-0.260	0.097

Homology model construction

The homology model of the protein: PfATP6 was built using Prime [17] accessible through the Maestro interface (Schrodinger, Inc.). All water molecules were removed and the bound ligand (TG) was kept for the template. During the homology model building Prime keeps the backbone rigid for the cases in which the backbone does not need to be reconstructed due to gaps in the alignment. The model was screened for unfavorable steric contacts and remodeled using a rotamer library database of Prime. Explicit hydrogen was added to the protein and the protein model was subjected to energy minimization using the Macromodel (Prime version 1.5) force-field OPLS-2005. Energy minimization and relaxation of the loop regions were performed using 300 iterations in a simple minimization method. The steepest descent energy minimization was carried out until the energy showed stability in the sequential repetition. Model evaluation was performed in PROCHECK v3.4.4 [18] producing plots which were analyzed for the overall and residue-by-residue geometry. Ramachandran plot [19] provided by the program PROCHECK assured very good confidence for the predicted protein. There were only 0.3% residues in the disallowed region and 0.9% residues in generously allowed regions. Nevertheless, PROCHECK assured the reliability of the structure and the protein was subjected to VERIFY3D [20] available from NIH MBI Laboratory Servers.

Table 4 11-Aza artemisinin derivatives with anti-malarial activities against the drug resistant malarial strain *P. falciparum* (W-2 clone) used in this work

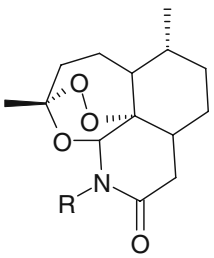

Sl. No.	R	Log RA	pIC_{50} (ng/ml)
71	C_3H_6Ph	0.020	0.283
72	C_2H_4Ph	0.160	0.439
73	C_5H_{11}	-0.200	0.121
74	CH_2(p-Cl-Ph)	-0.160	0.096
75	CH_2Ph	0.340	0.636
76	CH_2-(2-C_5H_4N)	1.460	1.487
77	2-Thiophene	0.170	0.458
78	Acetaldehyde	1.470	1.828

Ligand binding site prediction

Site directed mutagenesis study in catalytic site of PfATP6 of *Palsmodium falciparum* has revealed that Leu 263 is the critical residue involved in binding of artemisinin with PfATP6 [21]. In silico prediction of binding site was done for the PfATP6 in *P. falciparum* using SiteMap (Schrodinger package). SiteMap treats entire protein to locate binding sites whose size, functionality and extent of solvent exposure meet user specifications. SiteScore, the scoring function used to assess a site's propensity for ligand binding, accurately ranks possible binding sites to eliminate those not likely to be pharmaceutically relevant. It identifies potential ligand binding sites by linking together "site points" that are suitably close to the protein surface and sufficiently well sheltered from the solvent. The given similar terms dominate the site scoring function; this approach ensures that the search focuses on regions of the protein most likely to produce tight protein-ligand or protein-protein binding. Subsites are merged into larger sites when they are sufficiently close and could be bridged in solvent-exposed regions by ligand atoms. SiteMap evaluates sites using a series of properties. The binding site with highest site score was taken for docking of the artemisinin analogues. The binding pocket obtained by in silico studies on PfATP6 of *Plasmodium falciparum* was in consistent with the site directed mutagenesis studies. The algorithm proceeds as follows: the protein is projected onto a 3D grid with a step size of 1.0 Å; grid points are labeled as protein surface or solvent using certain rules. A grid point is marked in protein if there is at least one atom within 1.6 Å. After the solvent excluded surface was calculated the surface vertices' coordinates were stored. A sequence of grid points which starts and ends with the surface grid points which has solvent grid points in between is called a surface–solvent–surface event. If the number of surface–solvent–surface events of a solvent grid exceeds a minimal threshold of 6, then this grid is marked as a pocket.

Finally, all pocket grid points are clustered according to their spatial proximity. The clusters are ranked by the number of grid points in the cluster. The top three clusters are retained and their centers of mass are used to represent the predicted pocket sites.

Preparation of the ligands

An initial dataset of 150 artemisinin analogues were collected from published data [22–27] in which several different ring systems were represented. All of the analogues were either peroxides or trioxanes which should act *via* similar mechanisms of action and they were categorized into 10 classes (Tables 1, 2, 3, 4, 5, 6, 7, 8, 9, 10, 11 and 12). Each of these compounds had associated in vitro bioactivity values (IC_{50} values reported in ng/ml) against the drug resistant malaria strain *P. falciparum* (W-2 clone). The log value of the relative activity (RA) of these compounds was used for analysis and was defined as:

$$\mathrm{Log(RA)} = \log[(\text{artemisinin } IC_{50}/\text{analogue } IC_{50})(\text{analogue MW}/\text{artemisinin MW})].$$

Molecular models of the artemisinin and its analogues (Tables 1, 2, 3, 4, 5, 6, 7, 8, 9, 10, 11 and 12) were built using the builder feature in Maestro (Schrodinger package) and energy minimized in vacuum using Impact. Each structure was assigned an appropriate bond order using ligprep script shipped by Schrödinger and optimized initially by means of the OPLS 2005 force field using default setting. Complete geometrical optimization of these structures was carried out with the HF/3-21G method using the Jaguar (Schrodinger Inc.). In order to check the reliability of the geometry obtained we compared the structural parameters of the artemisinin 1,2,4-trioxane ring with theoretical [28] and experimental [29, 30] values from the literature. All calculations reproduced

Table 5 Artemisinin derivatives lacking the D-ring with anti-malarial activities against the drug resistant malarial strain *P. falciparum* (W-2 clone) used in this work

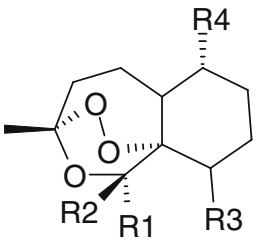

Sl. No.	R1	R2	R3	R4	Log RA	pIC_{50} (ng/ml)
79	$-O_2CCH_2Ph$	H	H	CH_3	-0.510	-0.217
80	H	H	H	CH_3	-0.320	0.202
81	H	OCH_3	H	H	-0.310	0.180
82	C_2H_4OH	H	CH_3		-1.800	-1.429
83	C_2H_4OH	CH_3	H		0.230	0.601
84	C_2H_4OH	CH3	CH3		-1.800	-1.449
85	$C_2H_4OCH_2Ph$	CH3	CH3		-1.800	-1.558
86	OCH_3	H	$C_2H_4O_2CNEt_2$	H	0.650	0.929
87	OCH_3	H	$C_2H_4O_2CNPh_2$		0.650	0.829
88	H	OCH_3	$C_2H_4OCH_2Ph$	H	0.750	1.039
89	H	OCH_3	C_2H_4O-allyl	H	0.400	0.735
90	H	OCH_3	$C_2H_4O_2Ph$	H	-0.590	-0.319
91	H	OCH_3	$C_2H_4O_2C(4\text{-}PhCO_2C_2H_4NMe_2)$		-0.600	-0.446
92	H	OCH_3	$C_2H_4O_2CCH_2NCO_2\text{-}(t\text{-}C_4H_9)$	H	-0.040	0.174
93	OCH_3	-	$C_2H_4OCH_2(4\text{-F-Ph})$		0.380	0.648
94	OCH_3	-	$C_2H_4OCH_2(4\text{-Py})$		0.140	0.428
95	H	OCH_3	$C_2H_4OCH_2(4\text{-N-Me-pyridine})$	H	-0.900	-0.647

Table 6 Miscellaneous artemisinin derivatives with anti-malarial activities against the drug resistant malarial strain *P. falciparum* (W-2 clone) used in this work

Sl. No.	Ligand structure	Log RA	pIC_{50} (ng/ml)
96	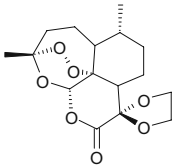	-2.090	-1.755
97	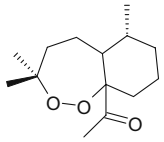	-1.270	-0.802
98	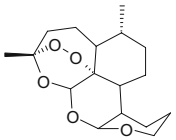	0.230	0.587
99	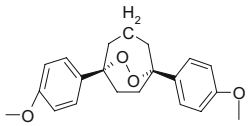	-0.670	-0.353
100	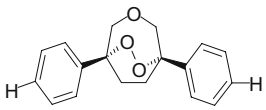	-2.260	-1.862
101	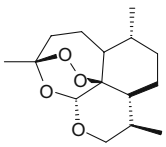	-0.240	0.180
102	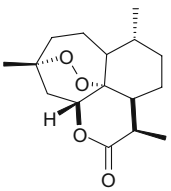	-0.960	-0.559
103	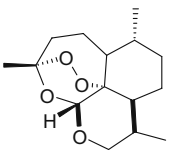	-0.790	-0.370
104	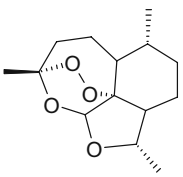	-0.353	0.090

most of the structural parameters of the artemisinin 1,2,4-trioxane ring seen in X-ray structures (Table 13). This applies especially to the bond length of the endoperoxide bridge which seems to be responsible for the antimalarial activity [31–34].

Docking of the ligands

All the ligands were docked to the PfATP6 receptor using Glide [35]. After ensuring that protein and ligands are in correct form for docking the receptor-grid files were

Table 7 9-substituted artemisinin derivatives with anti-malarial activities against the drug resistant malarial strain *P. falciparum* (W-2 clone) used in this work

Sl. No.	Ligand structure	Log RA	pIC_{50} (ng/ml)
105	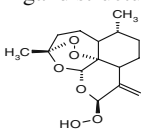	-0.739	-0.365
106	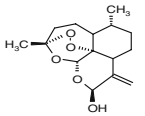	-2.219	-1.821
107	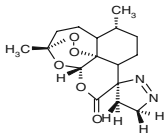	-2.447	-2.106
108	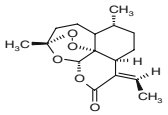	-0.198	0.182
109	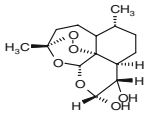	-0.717	-0.325
110	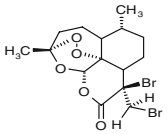	-1.487	-1.282
111	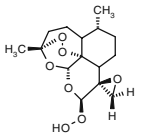	-0.460	-0.109
112	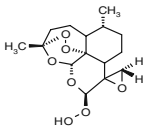	-0.409	-0.058
113	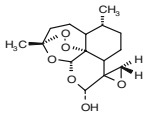	-0.361	0.013

generated using grid-receptor generation program using van der Waals scaling of the receptor at 0.4. The default size was used for the bounding and enclosing boxes. The ligands were docked initially using the "standard precision" method and further refined using "xtra precision" Glide algorithm. For the ligand docking stage van der Waals scaling of the ligand was set at 0.5. Of the 50,000 poses that were sampled, 4,000 were taken through minimization (conjugate gradients 1,000) and the 30 structures having the lowest energy conformations were further evaluated for the favorable Glide docking score [36]. A single best conformation for each ligand was considered for further analysis.

Table 8 Dihydroartemisinin derivatives with anti-malarial activities against the drug resistant malarial strain *P. falciparum* (W-2 clone) used in this work

Sl. No.	Ligand structure	Log RA	pIC_{50} (ng/ml)
114	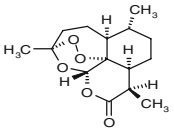	-0.269	0.129
115	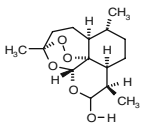	0.310	0.705
116	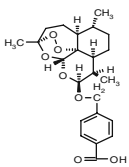	0.176	0.404
117	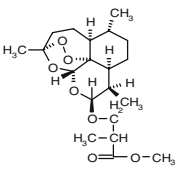	1.524	1.788
118	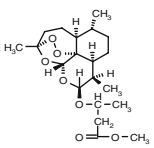	0.599	0.863

Ligand & structure-based descriptors (LSBD) protocol

The eMBrAcE and Prime MM-GBSA calculations were performed using the Ligand & Structure-Based Descriptors (LSBD) application of the Schrödinger software package.

Table 9 Tricyclic 1,2,4-trioxane derivatives with anti-malarial activities against the drug resistant malarial strain *P. falciparum* (W-2 clone) used in this work

Sl. No.	Ligand structure	Log RA	pIC_{50} (ng/ml)
119	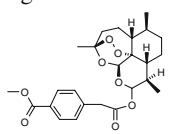	0.660	0.845
120	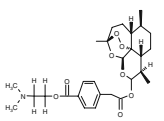	0.205	0.340
121	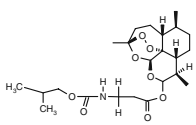	0.312	0.503

Table 10 N-alkyl-11-aza-9-desmethylartemisinin derivatives with anti-malarial activities against the drug resistant malarial strain *P. falciparum* (W-2 clone) used in this work

Sl. No.	Ligand structure	Log RA	pIC_{50} (ng/ml)
122	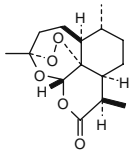	0.000	0.398
123	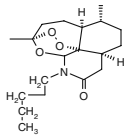	0.041	0.362
124	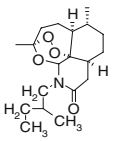	0.173	0.494
125	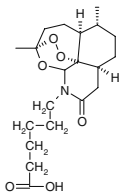	-0.921	-0.652
126	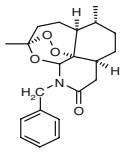	0.276	0.572
127	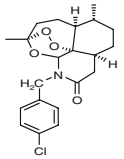	0.045	0.301
128	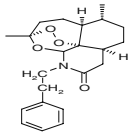	0.294	0.573
129	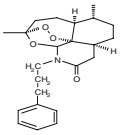	0.312	0.574

These calculations were applied to the ligand-receptor complex structures obtained from Glide docking.

Multi-ligand bimolecular association with energetics (eMBrAcE)

The eMBrAcE program calculates binding energies between ligands and receptors using molecular mechanics energy minimization for docked conformations. eMBrAcE applies multiple minimizations, during which each of the specified pre-positioned ligands is minimized with the receptor. For the energy-minimized structures, the calculation is performed first on the receptor ($E_{protein}$), then on the ligand (E_{ligand}), and finally on the complex ($E_{complex}$). The energy difference is then calculated as:

$$\Delta E = E_{complex} - E_{ligand} - E_{protein}$$

eMBrAcE uses the OPLS-AA all-atom force field with the surface generalized Born implicit solvent model [37, 38]. It uses traditional molecular mechanics (MM) methods to calculate ligand-receptor interaction energies (G_{ele}, G_{vdW}, G_{solv}) with a Gaussian smooth dielectric constant function method [39, 40] for electrostatic part of solvation energy and solvent-accessible surface for the nonpolar part of solvation energy. A conjugate gradient minimization protocol was used in all minimization. After all energies were calculated factor analysis (FA) and multiple regression analysis (MRA) were used to derive a LRE-like equation which could produces a reasonable free energy of binding (FEB) with the activity of these compounds.

Prime MM-GBSA

This application is used to predict the binding free energy between a receptor and a ligand. MM-GBSA is a method that combines OPLS molecular mechanics energies (E_{MM}), surface generalized Born solvation model for polar solvation (G_{SGB}), and a nonpolar solvation term (G_{NP}). The G_{NP} term comprises the nonpolar solvent accessible surface area and van der Waals interactions. The total free energy of binding is calculated as:

$$\Delta G_{bind} = G_{complex} - \left(G_{protein} + G_{ligand}\right)$$

$$G = E_{MM} + G_{SGB} + G_{NP}$$

In order to explore the reliability of the proposed model we used the cross validation method. Prediction error sum of squares (PRESS) is a standard index to measure the accuracy of a modeling method based on the cross validation technique. The r_{cv}^2 was calculated based on the PRESS and SSY (sum of squares of deviations of the experimental values from their mean) using the following formula:

$$r_{cv}^2 = 1 - \frac{PRESS}{SSY} = 1 - \frac{\sum_{i=1}^{n}\left(y_{\exp} - y_{pred}\right)^2}{\sum_{i=1}^{n}\left(y_{\exp} - \bar{y}\right)^2},$$

where y_{exp}, y_{pred} and $\bar{y}$ are the predicted, observed and mean values of the relative activities of the artemisinin analogues. The cross validation analysis performed by using the leave one out (LOO) method in which one compound is removed from the data set and its activity is predicted using the model derived from the rest of the data points.

Results and discussion

The atomic coordinates of PfATP6 for the organism *Plasmodium falciparum* was not available in Protein Data Bank which necessitated for developing a protein model. The final model, which we took for further analysis, consisted of 895 amino acid residues. We used both PROCHECK and VERIFY3D softwares to check the quality of the modeled protein. Ramachandran plot obtained from the program PROCHECK, which checks the stereochemical quality of a protein structures, producing a number of postscript plots analyzing its overall and residue-by-residue geometry, assured the reliability of the modeled protein with 91.1% residues in most allowed region and 7.7% in additional allowed region. There were only 0.3% residues in disallowed region and 0.9% in generously allowed region. The assessment with VERIFY3D, which derives a "3D-1D" profile based on the local environment of each residue, described by the statistical preferences for: the area of the residue that is buried, the fraction of side-chain area that is covered by polar atoms (oxygen and nitrogen) and the local secondary structure, also substantiated the reliability of the three dimensional structure. The residues that deviated from the standard conformational angles of Ramachandran plot were the members of N terminal domain of the protein. This was an ignorable condition since the N-terminal end was not critical in our study. The distance of these residues to the active site residues also were found to be more than 10 Å, which suggested that those residues would interfere little with the binding of ligands in the active site region of PfATP6. The structural comparison of template protein and PfATP6 modeled structure (Fig. 3) showed significant similarity in the binding site residues. Active site was identified with reference to the studies done on SERCA (pdb ID: 1IWO). We carried out in silico studies to confirm these active sites using SiteMap algorithm. The output from the Sitemap program (Fig. 4) showed coherent active sites for the target protein as reported in site directed mutagenesis study [21].

One of the key challenges in computer-aided drug discovery is to maximize the capabilities of the method in use for predicting and rank-ordering the binding affinities of compounds for a given target protein. The efficiency of a prediction method is predominantly determined by these capabilities. Various descriptors extracted from the structural information on ligand-receptor complex may provide an advantageous solution to create a reliable binding-affinity-prediction model. Here, we combined the results obtained from a standard docking protocol with the data from three different structure-based descriptors and then investigated the utility of these descriptors on the virtual screening efficiency for artemisinin derivatives.

Docking simulation of artemisinin derivatives to the homology modeled PfATP6 was performed using the Glide program (Schrodinger package). All the 150 artemisinin ligands with known antimalarial activities (W2 clone) and thapsigargin (TG) were docked into the defined binding site. The original crystal structure of TG was extracted from TG-SERCA complex (pdb ID: 1IWO) and was re-docked into the binding site of PfATP6 in order to validate the Glide-XP docking protocol. The top 10 configurations after docking were taken into consideration to validate the result (Table 14). The RMSD was calculated for each configuration in comparison to the co-crystallized TG and the value was found to be in between 0.02–0.85 Å. Whereas the RMSD value calculated out of ten accepted poses for each configuration was found in between 0.59–1.33 Å. This revealed that the docked configurations have similar binding positions and orientations within the binding site and are similar to the crystal structure. The best docked structures which are the configuration with the lowest Glide score is compared with the crystal structure as shown in Fig. 5. These docking results illustrated that thapsigargin in PfATP6 maintained the same spatial coordinates as in SERCA. Docking of artemisinin derivatives to this binding site was performed using the standardized docking protocol. The binding mode of both TG and artemisinin within the binding site is represented in Fig. 6. In this figure we can observe that both the molecules were well fitted to the defined binding pocket. All 150 artemisinin analogues were also found to be good binders with PfATP6. The binding modes of artemisinin and its derivatives showed hydrophobic interaction with PfATP6. This binding mode proved the hypothesis that the artemisinin derivatives bind to PfATP6 with almost hydrophobic interactions and it should be the preorganized shape binding between the rigid structure of artemisinin analogues and the binding pocket of PfATP6. As the Fe^{2+}-dependent activation and antimalarial activity of artemisinin do not depend on the heme binding [41], we can propose that the production of the carbon centered free radical [32] should not precede the binding to PfATP6. Therefore, artemisinin should be bound to PfATP6 before activation by Fe^{2+} ion. For each ligand in the virtual library, the pose with the lowest Glide score was rescored using Prime/MM-GBSA and eMBrAcE approaches. These approaches predict the binding free energy for a set of ligands to receptor.

Table 11 3C-substituted artemisinin derivatives with anti-malarial activities against the drug resistant malarial strain *P. falciparum* (W-2 clone) used in this work

Sl. No.	Ligand structure	Log RA	pIC50 (ng/ml)	Sl. No.	Ligand structure	Log RA	pIC50 (ng/ml)
130	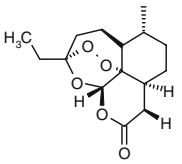	0.049	0.447	137	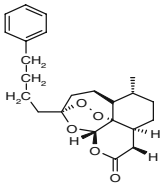	0.449	0.710
131	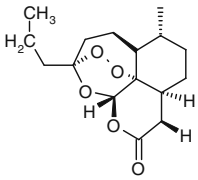	0.828	1.205	138	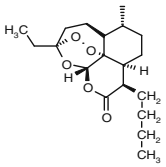	0.410	0.729
132	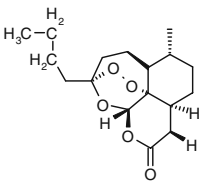	-0.745	-0.385	139	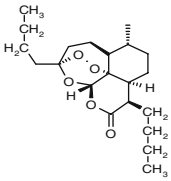	-0.481	-0.197
133	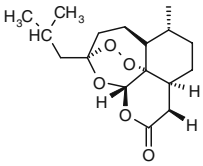	-0.347	0.010	140	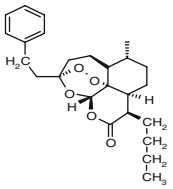	-2.000	-1.769
134	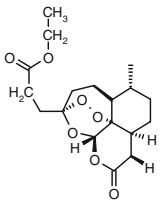	0.365	0.665	141	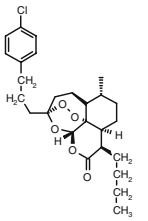	-0.276	-0.093
135	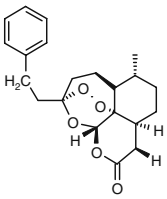	-2.000	-1.706	142	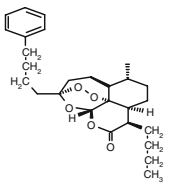	-0.319	-0.116
136	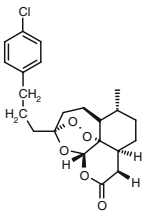	0.104	0.343	143	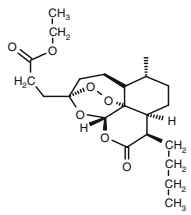	1.359	1.594

Table 12 Various derivatives of artemisinin and artemether with antimalarial activity against the drug resistant malarial strain *P. falciparum* (W-2 clone) used in the work

Compound no.	Analogue structure	Log RA	pIC_{50} (ng/ml)	Compound no.	Analogue structure	Log RA	pIC_{50} (ng/ml)
144	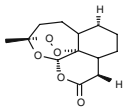	0.437	0.083	148	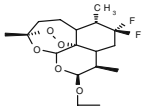	1.549	0.497
145	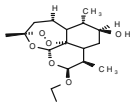	2.188	0.672	149	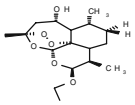	0.054	-0.938
146	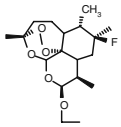	-0.120	0.192	150	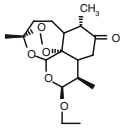	0.160	0.495
147	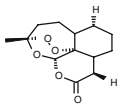	0.016	-1.347				

Building models for prediction of Log RA using Glide score and Prime/MM-GBSA energy

Prediction models for antimalarial activity were built by considering the Glide score and ΔG_{bind} as descriptors. The docking score and the ΔG_{bind} energy of the analogues are included in Table 15.

The Eq. 1 of the model and the corresponding statistics are shown below:

$$\text{Log RA} = -3.18(\pm 0.241) - 0.509(\pm 0.038) \times \text{G-score} \quad (1)$$

$$(\text{N} = 150; r^2 = 0.538; \text{s} = 0.601; \text{F} = 178.22; r^2_{cv} = 0.525;$$

$$\text{PRESS} = 56.811)$$

Table 13 Experimental and theoretical values of the 1,2,4-trioxane ring parameters in artemisinin (bond lengths in Å; bond angles and torsional angles in degrees)

Parameters[a]	Theoretical			Experimental[d]	Experimental[e]
	3-21G[b]	3-21G** [c]	6-31G[c]		
O1-O2	1.463	1.462	1.447	1.475(4)	1.469(2)
O2-C3	1.441	1.440	1.435	1.417(4)	1.416(3)
C3-O4	1.436	1.436	1.435	1.448(4)	1.445(2)
O4-C5	1.407	1.408	1.403	1.388(4)	1.379(2)
C5-C6	1.529	1.530	1.533	1.528(5)	1.523(2)
C6-O1	1.478	1.477	1.469	1.450(4)	1.461(2)
O1-O2-C3	106.9	107.070	108.800	107.600(2)	108.100(1)
O2-C3-O4	107.0	107.310	106.760	107.200(2)	106.600(2)
C3-O4-C5	115.6	115.700	117.300	113.500(3)	114.200(2)
O4-C5-C6	112.0	112.030	112.280	114.700(2)	114.500(2)
C5-C6-O1	111.1	111.589	110.910	111.100(2)	110.700(2)
C6-O1-O2	111.2	111.286	113.240	111.500(2)	111.200(2)
O1-O2-C3-O4	−74.9	−74.680	−71.840	−75.500(3)	−75.500(2)
O2-C3-O4-C5	31.8	32.150	33.390	36.300(4)	36.000(2)
C3-O4-C5-C6	29.4	28.400	25.320	24.800(4)	25.300(2)
O4-C5-C6-O1	−51.8	−50.769	−49.410	−50.800(4)	−51.300(2)
C5-C6-O1-O2	10.1	9.792	12.510	12.300(3)	12.700(2)
C6-O1-O2-C3	50.8	50.522	46.700	47.700	47.800(2)

[a] Atoms are numbered according to Fig. 1

[b] This work

[c] Values from Ref. [28]

[d] Values from Ref. [29] (experimental estimated standard deviations in brackets)

[e] Values from Ref. [30] (experimental estimated standard deviations in brackets)

**Represents the polarization functions on all the atoms except the transition metal ions which is used in the basis set 3-21G for optimization of structure

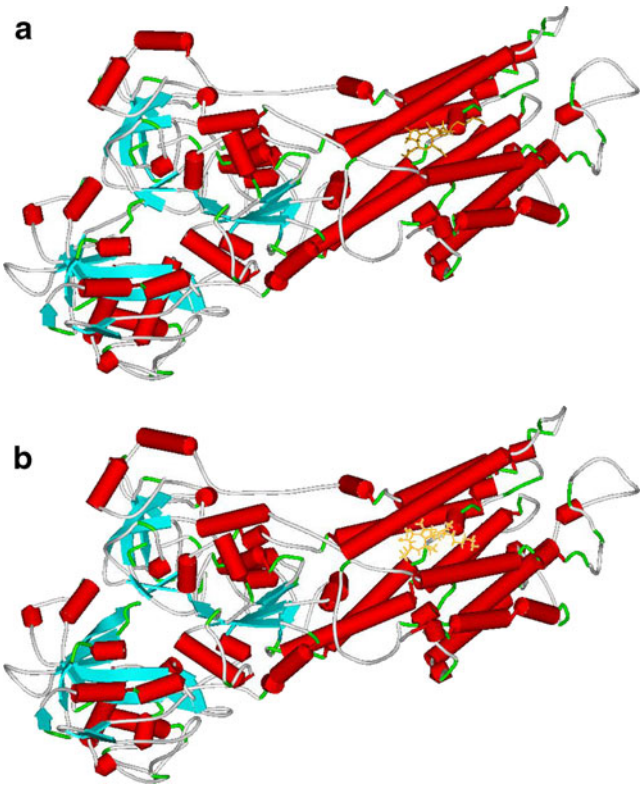

Fig. 3 Schematic display of (**a**) SERCA (above) and (**b**) PfATP6 (below) generated using DS Visualizer for windows. Helices and sheets are represented as red cylinders and cyan arrows, respectively. The ligand TG (in brown stick) is included in the structure

The root mean square error (RMSE) between the experimental RA and the predicted RA obtained by the regression model was 0.524 which is an indicator of the robustness of the fit and suggested that the calculated RA based on Glide score is reliable. The quality of the fit can also be judged by the value of the squared correlation coefficient (r^2), which was 0.538 for the data set. Figure 7 graphically shows the quality of fit. The statistical significance of the prediction model is evaluated by the correlation coefficient r^2, standard error, F-test value, leave-one-out cross-validation coefficient r^2_{cv} and predictive error sum of squares PRESS. The regression model developed in this study is statistically ($r^2_{cv} = 0.525$, r^2=0.538, F=178.22) best fitted and consequently used for prediction of antimalarial activities (log RA) of the artemisinin analogues as reported in Table 15.

We have used Prime/MM-GBSA protocol for rescoring Glide XP poses of the artemisinin analogues. We did find a better correlation between ΔG_{bind} energy and experimental RA (r^2=0.688) (Fig. 8). Rescoring using Prime/MM-GBSA leads to minor changes of the ligand conformations (due to energy minimization of the ligand in receptor's environment) and consequent stabilization of receptor and ligand complex. A linear regression model for prediction of predicted antimalarial activity (log RA) has been developed by considering analogues with known experimental activity. In this model we have taken ΔG_{bind} energy as a descriptor. The Eq. 2 of the model and the corresponding statistics are shown below:

$$\text{Log RA} = -1.66(\pm 0.098) - 0.102(\pm 0.006) \times \Delta G_{bind} \quad (2)$$

$$(N = 150; r^2 = 0.688; s = 0.495; F = 333.24; r^2_{cv} = 0.679;$$

$$\text{PRESS} = 37.997).$$

The regression model developed based on ΔG_{bind} energy is statistically ($r^2_{cv} = 0.679$, r^2=0.688, F=333.24) best fitted and consequently used for prediction of antimalarial activities (log RA) of the artemisinin analogues as reported in Table 15. The average root mean square error between predicted and experimental RA values was found to be 0.445 by using leave-one-out cross validation technique which further revealed the reliability of the model for prediction of antimalarial activity. However, we may observe that model using ΔG_{bind} descriptor is better for predicting antimalarial activity than model using Glide score as a descriptor.

Linear optimization of energy parameters *vs.* activity

One docking structure with better Glide score from each molecule docking result was picked up as final docked structure in PfATP6 for further calculations. As the Glide program treats a receptor rigidly during docking simulation an energy minimization was performed to the docked complex. The vdW energy and electrostatic energy between ligand and

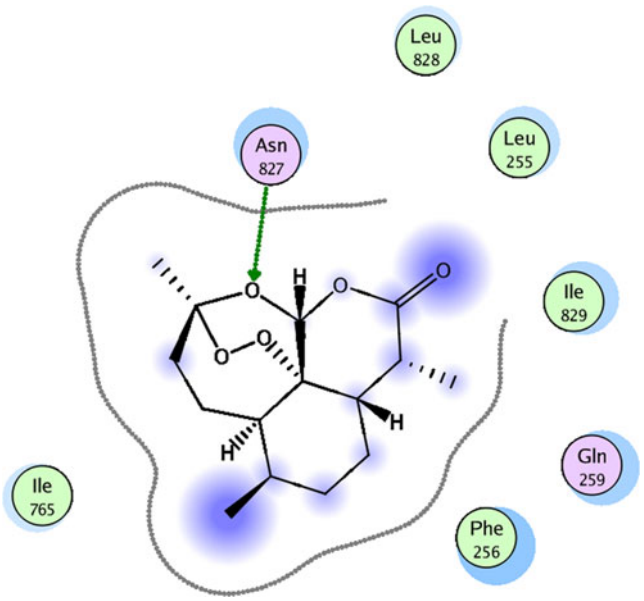

Fig. 4 Ligplot of PfATP6- artemisinin binding site along with artemisinin

Table 14 The RMSD and docking score from the docking simulation of 10 lowest configurations of crystal structure of TG with PfATP6

Configuration	Glide score	ΔG_{score} [a]	RMSD [b] (Å)	RMSD [c] (Å)
1	−9.33	0	0.37	0.04
2	−9.28	1.24	0.53	0.05
3	−8.04	1.29	0.57	0.02
4	−8.02	1.31	0.74	0.03
5	−8.01	1.32	0.81	0.02
6	−7.93	1.4	0.85	0.02
7	−7.53	1.8	1.02	0.02
8	−7.33	2.0	1.27	0.02
9	−6.99	2.34	1.36	0.01
10	−6.41	2.92	1.57	0.05

[a] $\Delta G_{score} = E_i - E_{lowest}$, [b] RMSD, RMSD between docked and crystallographic thapsigargin structure, [c] RMSD, RMSD between docked poses corresponding to each configuration

receptor were calculated for each minimized complex. Also desolvation energy and solvent accessible surface area (SASA) change was calculated using eMBrAcE (Schrodinger package). All these energies are listed in Table 16. By graphing these energies *vs*. activity (log RA) of these ligands all have bad correlation to experimental activity of the set of ligands. SASA has some degree correlation to activity for some subset ligands. A scheme similar to linear response was used to develop a free energy of binding (FEB) relationship based on these energies which can express the activity of these artemisinin derivatives. A multiple regression was performed using Minitab statistical package. The properties of the final regression model are listed in Table 17. From the results of correlation factor analysis it can be seen that ΔG_{vdW} has most significant correlation to the activity (log RA) and electrostatic energy (ΔGele) has less significant correlation. It indicates that the binding of these artemisinin derivatives to PfATP6 is almost hydrophobic. ΔG_{vdW} may be a major driving force to their binding.

The predicted activity (log RA) of these artemesinin derivatives are listed in Table 16. The correlation between predicted activity and actual activity is shown in Fig. 9. The calculated activity has good correlation to the actual activity. The linear optimization of energy parameters represents the actual activity very well. Theoretically, the binding affinity of drug molecules can be partitioned into several components: vdW, electrostatic, solvation and entropy. Generally the entropy is the most difficult component to calculate. Different methods have been suggested to estimate the entropy contribution. To relative rigid molecules the entropy is relatively small and normally ignored or cancelled in relative free energy calculation. In the rational drug design the calculation of relative binding free energy rather than absolute binding free energy is normally pursued. Several papers have been reported on reasonable correlation between calculated FEB and activity for a small set of ligands. Although these energy components are added directly

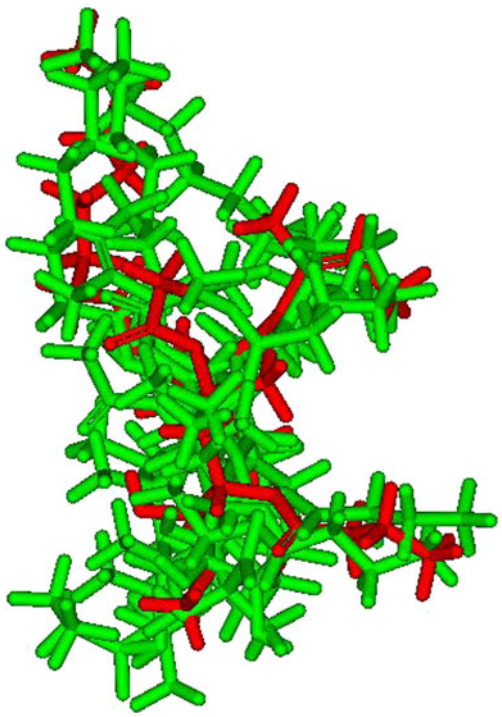

Fig. 5 Superposition of all docked configurations of TG on crystal structure (*red-stick*). RMSD (heavy atom)=0.37–1.57 Å

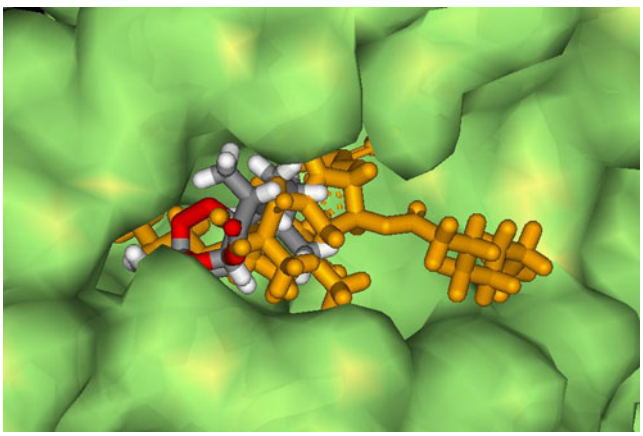

Fig. 6 Binding mode of artemisinin and TG within the binding site of PfATP6. TG: brown stick model and Artemisinin: gray stick model

Table 15 Predicted antimalarial activities of (a) analogues using Glide score (XP) and Prime/MM-GBSA energy as a descriptor and experimental activity

Ligand	Glide Score	ΔG_{bind} (kcal/mol)	Expt. Log RA	[a]Pred. Log RA (Gscore)	[b]Pred. Log RA (ΔG_{bind})
(a) Artemisinin derivatives					
1	−6.62	−20.21	1.00	0.19	0.40
2	−5.25	−12.66	0.45	−0.51	−0.37
3	−4.16	−10.00	−1.10	−1.06	−0.64
4	−6.37	−28.32	0.79	0.06	1.23
5	−6.56	−12.27	−0.60	0.16	−0.41
6	−6.28	−12.14	−0.10	0.02	−0.42
7	−7.50	−23.47	0.17	0.64	0.73
8	−7.25	−17.19	−0.32	0.51	0.09
9	−7.67	−12.10	−0.28	0.72	−0.43
10	−7.27	−24.49	1.36	0.52	0.84
11	−7.74	−26.16	1.40	0.76	1.01
12	−7.11	−22.75	0.86	0.44	0.66
13	−6.18	−18.36	−0.55	−0.03	0.21
14	−7.17	−12.49	−0.04	0.47	−0.39
15	−6.80	−18.99	−0.04	0.28	0.28
16	−6.88	−22.64	0.07	0.32	0.65
17	−6.28	−14.73	0.37	0.01	−0.16
18	−5.47	−12.79	0.05	−0.40	−0.36
19	−6.28	−19.12	0.83	0.01	0.29
20	−8.20	−28.54	1.37	0.99	1.25
21	−5.16	−20.63	−0.36	−0.56	0.44
22	−6.54	−27.74	1.02	0.15	1.17
23	−7.26	−17.00	0.63	0.51	0.07
24	−7.68	−16.62	0.12	0.73	0.04
25	−7.86	−21.75	0.78	0.82	0.56
(b) 10-Substituted artemisinin derivatives					
26	−6.10	−17.61	0.75	−0.08	0.14
27	−5.61	−18.11	0.55	−0.32	0.19
28	−5.57	−11.91	0.34	−0.35	−0.45
29	−6.96	−28.89	0.96	0.36	1.29
30	−5.10	−5.53	−1.08	−0.58	−1.10
31	−7.85	−22.45	0.28	0.82	0.63
32	−6.51	−21.46	0.66	0.13	0.53
33	−7.38	−12.05	0.18	0.58	−0.43
34	−7.28	−17.18	−0.09	0.52	0.09
35	−6.78	−8.39	−0.77	0.27	−0.80
36	−6.76	−21.43	0.28	0.26	0.53
37	−8.03	−23.15	0.32	0.91	0.70
38	−7.40	−27.96	1.32	0.59	1.19
39	−8.24	−20.83	0.67	1.01	0.46
40	−7.79	−20.43	−0.04	0.78	0.42
41	−8.32	−16.40	0.50	1.05	0.01
42	−5.92	−16.69	0.78	−0.17	0.04
43	−7.95	−15.18	0.52	0.87	−0.11
44	−6.84	−16.97	0.10	0.30	0.07
45	−6.53	−10.43	−0.03	0.14	−0.60
46	−5.49	−8.64	−0.07	−0.39	−0.78

Table 15 (continued)

Ligand	Glide Score	ΔG_{bind} (kcal/mol)	Expt. Log RA	[a]Pred. Log RA (Gscore)	[b]Pred. Log RA (ΔG_{bind})
47	−8.24	−29.13	1.79	1.01	1.31
48	−8.88	−28.91	2.18	1.34	1.29
49	−6.55	−21.56	0.87	0.15	0.54
50	−7.98	−28.76	1.70	0.88	1.27
51	−6.68	−15.59	0.70	0.22	−0.07
52	−7.09	−14.27	−0.55	0.43	−0.20
53	−5.99	−26.30	0.75	−0.13	1.02
54	−5.36	−11.18	−1.00	−0.45	−0.52
55	−5.67	−15.15	0.40	−0.29	−0.11
56	−6.72	−18.20	0.84	0.24	0.20
57	−7.67	−14.17	0.58	0.72	−0.21
58	−5.30	−17.61	−0.57	−0.48	0.14
59	−5.59	−12.91	−0.99	−0.33	−0.34
60	−5.40	−13.48	−0.89	−0.43	−0.29
61	−6.98	−13.50	0.16	0.38	−0.28
62	−7.31	−25.49	1.40	0.54	0.94
63	−6.41	−28.33	0.74	0.08	1.23
64	−6.13	−23.29	0.33	−0.06	0.72
65	−5.38	−14.84	−0.70	−0.44	−0.15
66	−6.14	−8.72	−0.44	−0.06	−0.77
67	−6.45	−22.30	0.92	0.10	0.61
(c) Seco-artemisinin derivatives					
68	−3.33	−1.26	−2.37	−1.49	−1.53
69	−4.68	−5.91	−1.13	−0.80	−1.06
70	−5.59	−20.41	−0.26	−0.33	0.42
(d) 11-Aza artemisinin derivatives					
71	−6.31	−15.84	0.02	0.03	−0.04
72	−7.66	−13.00	0.16	0.72	−0.33
73	−5.84	−14.60	−0.20	−0.21	−0.17
74	−5.35	−11.67	−0.16	−0.46	−0.47
75	−6.10	−16.28	0.34	−0.07	0.00
76	−7.78	−27.77	1.46	0.78	1.17
77	−5.14	−23.04	0.17	−0.56	0.69
78	−8.00	−27.17	1.47	0.89	1.11
(e) Artemisinin derivatives lacking the D-ring					
79	−7.36	−8.13	−0.51	0.56	−0.83
80	−6.19	−7.71	−0.32	−0.03	−0.87
81	−5.97	−12.73	−0.31	−0.14	−0.36
82	−3.56	−4.78	−1.80	−1.37	−1.17
83	−5.30	−14.26	0.23	−0.48	−0.21
84	−3.91	−3.66	−1.80	−1.19	−1.29
85	−3.74	−3.88	−1.80	−1.28	−1.26
86	−5.95	−19.29	0.65	−0.15	0.31
87	−8.42	−17.92	0.65	1.11	0.17
88	−6.30	−22.34	0.75	0.02	0.62
89	−6.52	−14.00	0.40	0.14	−0.23
90	−6.75	−16.35	−0.59	0.26	0.01
91	−6.67	−6.14	−0.60	0.22	−1.03
92	−5.74	−8.81	−0.04	−0.26	−0.76

Table 15 (continued)

Ligand	Glide Score	ΔG_{bind} (kcal/mol)	Expt. Log RA	[a]Pred. Log RA (Gscore)	[b]Pred. Log RA (ΔG_{bind})
93	−7.15	−25.27	0.38	0.46	0.92
94	−5.72	−14.82	0.14	−0.27	−0.15
95	−6.55	−13.79	−0.90	0.15	−0.25
(f) Miscellaneous artemisinin derivatives					
96	−3.33	−1.30	−2.09	−1.49	−1.53
97	−4.45	−8.39	−1.27	−0.91	−0.80
98	−6.33	−14.42	0.23	0.04	−0.19
99	−5.84	−16.94	−0.67	−0.21	0.07
100	−3.20	−1.43	−2.26	−1.55	−1.51
101	−4.73	−9.31	−0.24	−0.77	−0.71
102	−5.03	−11.61	−0.96	−0.62	−0.48
103	−5.04	−11.09	−0.79	−0.62	−0.53
104	−4.62	−20.00	−0.35	−0.83	0.38
(g) 9-substituted artemisinin derivatives					
105	−4.38	−6.79	−1.49	−0.95	−0.97
106	−4.96	−6.29	−0.46	−0.66	−1.02
107	−5.55	−10.90	−0.41	−0.35	−0.55
108	−5.71	−18.53	−0.36	−0.28	0.23
109	−5.64	−12.88	−0.74	−0.31	−0.35
110	−3.62	−2.11	−2.22	−1.34	−1.44
111	−3.17	−0.56	−2.45	−1.57	−1.60
112	−5.25	−19.30	−0.20	−0.51	0.31
113	−5.76	−14.00	−0.72	−0.25	−0.23
(h) Dihydroartemisinin derivatives					
114	−5.04	−11.92	−0.27	−0.62	−0.44
115	−5.70	−21.73	0.31	−0.28	0.56
116	−6.37	−12.91	0.18	0.06	−0.34
117	−7.35	−26.00	1.52	0.56	0.99
118	−6.03	−23.09	0.60	−0.11	0.70
(i) Tricyclic 1,2,4-trioxane derivatives					
119	−7.88	−27.37	0.66	0.83	1.13
120	−8.16	−24.67	0.21	0.97	0.86
121	−8.30	−13.42	0.31	1.04	−0.29
(j) N-alkyl-11-aza-9-desmethylartemisinin derivatives					
122	−5.10	−21.65	0.00	−0.58	0.55
123	−6.37	−10.45	0.04	0.06	−0.59
124	−5.45	−16.18	0.17	−0.41	−0.01
125	−5.95	−6.54	−0.92	−0.15	−0.99
126	−6.89	−16.82	0.28	0.33	0.06
127	−5.61	−12.99	0.05	−0.32	−0.34
128	−6.73	−20.51	0.29	0.24	0.43
129	−6.48	−15.26	0.31	0.12	−0.10
(k) 3C-substituted artemisinin derivatives					
130	−5.15	−22.00	0.05	−0.56	0.58
131	−6.53	−20.00	0.83	0.14	0.38
132	−6.54	−15.43	−0.74	0.15	−0.09
133	−6.24	−19.37	−0.35	−0.01	0.32
134	−5.19	−24.15	0.37	−0.54	0.80
135	−3.50	−2.68	−2.00	−1.40	−1.39

Table 15 (continued)

Ligand	Glide Score	ΔG_{bind} (kcal/mol)	Expt. Log RA	[a]Pred. Log RA (Gscore)	[b]Pred. Log RA (ΔG_{bind})
136	−8.47	−24.36	0.37	1.13	0.82
137	−6.98	−24.72	0.45	0.37	0.86
138	−7.51	−9.22	−0.43	0.64	−0.72
139	−5.79	−4.78	−0.92	−0.23	−1.17
140	−6.89	−25.68	0.41	0.33	0.96
141	−6.31	−19.12	−0.48	0.03	0.29
142	−3.76	−1.80	−2.00	−1.27	−1.48
143	−7.64	−8.32	−0.28	0.71	−0.81
(l) Various derivatives of artemisinin and artemether					
144	−7.15	−8.89	−0.36	0.46	−0.75
145	−5.37	−12.07	0.34	−0.44	−0.43
146	−3.61	−5.03	−1.79	−1.34	−1.15
147	−5.07	−14.17	0.19	−0.60	−0.21
148	−4.30	−4.21	−1.27	−0.99	−1.23
149	−5.51	−9.81	−0.12	−0.37	−0.66
150	−4.79	−14.26	0.16	−0.74	−0.21

together in most of these applications it is still a challenge to apply these methods to a large set of ligands. Normally, these different energy components (vdW, electrostatic, solvation) were calculated using more than one method. To the same set of structure the use of different force fields or different methods will produce different values of energy. This suggests that these energy components need to be scaled before an equation is obtained to get a better expression for these energy components. A set of weights can be used to get free energy expression by linearly combining these energies. In this work a linear combination strategy was used to express FEB by four energy components calculated from different methods. An expression of free energy, whose weight coefficients were optimized by a multiple regression, was obtained and successfully predicted the activity of a large set of ligands. As stated earlier, the major interest in drug design is to express the variance of free energy over a set of active molecules. In this study the ΔG_{vdW} is the biggest contribution; SASA is the next contributor; electrostatic part and electrostatic part of solvation are the smallest contributor to the free energy variance. Equation 3 of the model and the corresponding statistics are shown below:

$$\text{Log RA} = -1.37 - 0.0035\ \text{SASA} - 0.0314\ \Delta G_{vdW} + 0.0029\ \Delta G_{ele} - 0.00398\ \Delta G_{solv} \quad (3)$$

$$(\text{N} = 150; r^2 = 0.815; \text{s} = 0.291; \text{F} = 141.99; r^2_{cv} = 0.802; \text{PRESS} = 11.65).$$

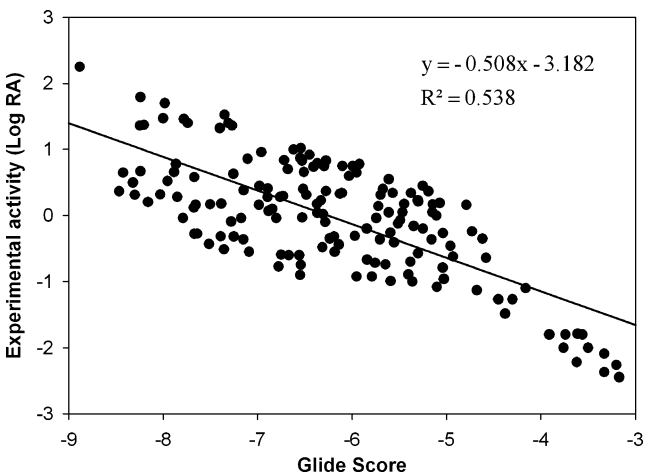

Fig. 7 Models for predicting antimalarial activity (Log RA) of the artemisinin derivatives based on Glide score

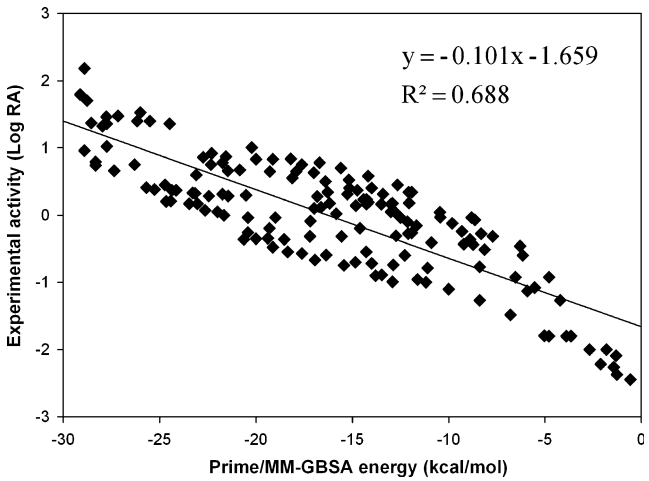

Fig. 8 Models for predicting antimalarial activity (Log RA) of the artemisinin derivatives based on Prime/MM-GBSA energy (ΔG_{bind})

Table 16 Predicted antimalarial activities of artemisinin derivatives based on linear response scheme of energy parameters and experimental activities for selected analogues

Sl. No.	SASA	ΔG_{vdW}	ΔG_{ele}	ΔG_{solv}	Log RA	[a]Log RA_{pred}
(a) Artemisinin derivatives						
1	459.0	−122.2	−116.4	106.2	1.00	1.02
2	624.5	−120.4	−97.4	104.9	0.45	0.01
3	591.7	−92.2	−138.6	118.4	−1.10	−0.69
5	512.5	−93.3	−66.3	65.4	−0.60	−0.16
6	436.8	−80.5	−87.7	103.2	−0.10	−0.12
7	633.3	−123.8	−31.7	87.8	0.17	0.09
8	690.3	−117.3	−29.0	61.4	−0.32	−0.44
9	741.4	−131.4	−123.1	144.6	−0.28	−0.35
12	609.6	−144.1	−203.2	199.6	0.86	0.76
13	521.3	−90.4	−152.6	127.5	−0.55	−0.34
14	477.4	−96.5	−36.5	66.4	−0.04	0.16
15	635.7	−119.6	−18.5	48.2	−0.04	−0.04
16	543.8	−105.0	−152.5	136.8	0.07	−0.03
17	475.0	−109.6	−76.8	90.1	0.37	0.56
18	479.9	−95.2	−94.7	61.0	0.05	0.08
19	508.2	−120.5	−48.3	83.0	0.83	0.71
20	654.6	−163.8	−77.2	107.1	1.37	1.17
21	521.8	−101.5	−80.9	95.7	−0.36	0.03
22	584.6	−142.0	−121.9	132.7	1.02	0.89
23	670.0	−141.4	−110.3	125.6	0.63	0.38
24	622.9	−119.5	−190.1	196.0	0.12	−0.06
25	647.4	−141.9	14.6	47.6	0.78	0.59
(b) 10-Substituted artemisinin derivatives						
26	497.3	−131.1	−133.6	120.4	0.75	1.06
27	475.3	−121.6	−93.8	85.2	0.55	0.92
28	663.6	−144.5	−670.9	620.4	0.34	0.20
29	574.3	−143.0	−221.9	198.8	0.96	0.93
30	532.7	−77.5	−68.6	59.1	−1.08	−0.76
31	637.0	−137.3	−41.0	63.3	0.28	0.48
32	532.3	−132.2	−47.9	56.8	0.66	0.93
33	574.9	−96.4	−121.2	103.3	0.18	−0.45
34	620.6	−126.7	−61.8	119.3	−0.09	0.24
35	654.1	−103.1	−68.0	76.2	−0.77	−0.68
36	711.9	−139.5	−134.4	156.8	0.28	0.06
37	694.7	−139.9	−183.3	205.5	0.32	0.15
38	674.6	−143.8	−67.2	137.1	1.32	1.03
39	827.3	−171.1	20.8	38.8	0.67	0.45
40	529.9	−111.2	−56.1	85.0	−0.04	0.30
41	658.8	−127.6	−168.1	165.6	0.50	−0.01
42	568.1	−131.4	−63.7	77.8	0.78	0.69
43	702.2	−141.0	−62.6	87.5	0.83	0.20
44	678.0	−126.2	−16.7	38.6	0.10	−0.08
45	688.1	−121.9	−42.0	57.6	−0.03	−0.29
46	669.7	−120.7	−34.1	62.1	−0.07	−0.21
47	681.1	−125.4	−15.0	57.2	1.79	1.53
48	551.1	−155.4	−106.0	77.2	2.18	1.84
49	504.0	−126.6	−51.9	69.0	0.87	0.92

Table 16 (continued)

Sl. No.	SASA	ΔG_{vdW}	ΔG_{ele}	ΔG_{solv}	Log RA	[a]Log RA_{pred}
50	631.1	−105.4	−47.0	67.2	1.70	1.48
51	575.1	−110.1	−42.9	54.4	0.70	0.01
52	673.1	−113.1	−38.7	97.9	−0.55	−0.47
53	536.8	−112.7	−109.5	107.7	0.75	0.27
54	581.8	−88.5	−22.5	45.5	−1.00	−0.68
55	501.5	−116.3	−33.5	35.7	0.40	0.63
56	512.4	−124.2	−107.3	98.8	0.84	0.77
57	659.9	−124.9	−56.1	118.8	0.58	−0.04
58	531.8	−96.8	−48.5	58.3	−0.57	−0.15
59	501.3	−77.6	−100.7	78.9	−0.99	−0.59
60	485.2	−72.4	−180.9	141.2	−0.89	−0.70
61	582.2	−105.5	−123.8	124.3	0.16	−0.22
62	627.7	−151.3	−17.9	70.3	1.40	0.98
63	521.1	−75.4	−34.0	41.2	0.71	0.49
64	535.3	−104.1	−76.4	56.7	0.33	0.04
65	548.8	−92.5	42.8	−12.0	−0.70	−0.33
66	548.9	−107.8	−78.7	88.1	−0.44	0.07
67	492.7	−117.8	−168.6	117.6	0.92	0.66
(c) Seco-artemisinin derivatives						
68	419.9	−46.7	−63.0	86.8	−2.37	−2.51
69	459.9	−56.6	−113.0	119.8	−1.13	−1.00
70	542.4	−118.8	−83.9	98.3	−0.26	0.44
(d) 11-Aza artemisinin derivatives						
71	651.8	−119.3	−77.7	119.6	0.02	−0.18
72	623.5	−119.2	−55.8	82.3	0.16	0.00
73	606.9	−119.2	−179.5	148.0	−0.20	0.03
74	628.8	−108.7	−14.2	47.2	−0.16	−0.33
75	581.9	−137.1	25.6	3.4	0.34	0.83
76	616.5	−157.6	−255.6	161.6	1.46	1.12
77	551.0	−118.1	−0.5	57.0	0.17	0.41
(e) Artemisinin derivatives lacking the D-ring						
78	592.5	−107.8	−68.6	74.6	1.47	1.64
79	611.6	−104.3	−360.5	411.6	−0.51	−0.57
80	418.9	−73.7	−87.9	77.2	−0.32	−0.22
81	419.0	−85.3	−73.7	94.6	−0.31	0.14
82	527.2	−52.5	−39.8	43.5	−1.80	−1.48
83	522.8	−116.9	−89.4	89.8	0.23	0.50
84	558.1	−63.0	−16.8	35.1	−1.80	−1.33
85	688.8	−136.4	−64.7	75.1	0.65	0.14
86	754.9	−144.2	−43.6	72.5	0.65	0.01
87	759.8	−133.6	−49.8	68.5	0.65	0.53
88	649.3	−129.9	−32.6	60.0	0.75	0.19
89	606.3	−115.5	−107.9	138.4	0.40	−0.05
90	659.8	−113.6	−59.8	69.5	−0.59	−0.39
91	874.4	−158.0	−480.8	531.2	−0.60	−0.51
92	695.1	−117.5	−159.8	155.8	−0.04	−0.53
93	657.1	−129.3	−74.0	89.3	0.38	0.10
94	611.3	−112.3	−37.5	54.2	0.14	−0.13
95	701.5	−102.6	−63.1	90.8	−0.90	−0.97

Table 16 (continued)

Sl. No.	SASA	ΔG_{vdW}	ΔG_{ele}	ΔG_{solv}	Log RA	[a]Log RA_{pred}
(f) Miscellaneous artemisinin derivatives						
96	481.6	−59.6	−85.1	93.3	−1.27	−1.02
97	492.7	−106.4	−56.2	66.9	0.23	0.37
98	612.7	−91.5	−107.1	132.5	−0.67	−0.82
99	618.4	−114.3	−160.5	211.6	−0.67	−0.37
100	473.8	−92.0	−87.8	79.1	−0.24	0.02
101	486.5	−75.2	−61.5	77.4	−0.96	−0.56
102	472.5	−75.3	−59.8	75.1	−0.79	−0.47
103	444.9	−91.8	−54.5	67.1	−0.35	0.20
(g) 9-substituted artemisinin derivatives						
104	516.9	−83.7	−77.9	87.2	−0.35	−0.72
105	508.1	−58.0	−155.3	151.3	−1.49	−1.26
106	484.3	−86.2	−142.6	135.4	−0.46	−0.25
107	490.3	−89.4	−141.0	131.1	−0.41	−0.19
108	470.1	−98.0	−144.3	153.8	−0.36	0.19
109	472.4	−73.5	−107.6	91.5	−0.74	−0.55
110	591.6	−69.6	−113.1	193.3	−2.22	−2.08
111	501.6	−73.4	−105.1	94.8	−2.45	−2.19
112	498.2	−101.8	−106.8	107.2	−0.20	0.17
113	464.5	−78.1	−159.8	174.5	−0.72	−0.40
(h) Dihydroartemisinin derivatives						
114	469.7	−106.4	−104.5	98.6	−0.27	0.48
115	472.4	−114.4	−72.1	48.6	0.31	0.72
116	465.8	−108.6	−22.2	43.4	0.49	0.61
117	651.1	−155.4	6.0	27.2	1.52	0.98
118	649.6	−147.6	−37.2	52.0	0.60	0.73
(i) Tricyclic 1,2,4-trioxane derivatives						
119	699.3	−141.2	−196.5	230.3	0.66	0.15
120	857.5	−162.5	−199.5	240.9	0.21	−0.12
121	765.0	−149.8	−194.1	199.7	0.31	0.04
(j) N-alkyl-11-aza-9-desmethylartemisinin derivatives						
122	473.4	−115.9	−63.4	70.2	0.00	0.77
123	578.7	−136.5	−98.0	142.1	0.04	0.76
124	591.5	−103.8	−44.3	46.9	0.17	−0.28
125	646.4	−109.2	−689.3	646.8	−0.92	−0.79
126	596.0	−136.6	−10.8	83.5	0.28	0.71
127	610.1	−141.0	−16.8	44.5	0.05	0.76
128	637.4	−131.4	−103.0	120.6	0.29	0.27
129	664.3	−128.2	−135.7	145.8	0.31	−0.01
(k) 3C-substituted artemisinin derivatives						
130	482.0	−112.9	−83.1	100.7	0.05	0.61
131	513.0	−121.3	−44.4	78.5	0.83	0.71
132	543.2	−87.5	−109.1	118.5	−0.74	−0.54
133	530.4	−102.0	−76.2	88.0	−0.35	0.00
134	610.6	−130.5	−174.8	185.1	0.37	0.35
135	581.6	−109.6	−125.3	143.7	−2.0	−1.68
136	642.6	−144.0	−23.4	65.6	0.37	0.66
137	622.4	−131.5	−250.5	252.9	0.45	0.28
138	812.2	−148.7	−325.0	396.0	−0.43	−0.35

Table 16 (continued)

Sl. No.	SASA	ΔG_{vdW}	ΔG_{ele}	ΔG_{solv}	Log RA	[a]Log RA_{pred}
139	786.8	−117.3	−324.9	413.9	−0.92	−1.17
140	657.1	−129.4	−62.1	86.6	0.41	0.94
141	547.5	−163.9	−78.9	94.9	−0.48	−0.47
142	593.5	−128.4	−151.0	136.0	0.41	0.40
143	619.9	−129.3	−79.7	107.3	−0.48	0.32
(l) Various derivatives of artemisinin and artemether						
144	435.4	−78.8	−141.0	151.5	−0.36	−0.20
145	555.6	−104.8	68.7	−45.2	0.34	0.02
146	567.1	−100.2	−78.1	58.3	−0.12	−0.27
147	531.8	−101.4	−65.7	57.8	0.16	−0.02
148	564.4	−104.7	−87.6	68.9	0.21	−0.12
149	554.0	−101.9	−54.6	42.3	0.19	−0.12
150	521.7	−73.3	−46.3	64.5	−1.27	−0.81

[a] Predicted RA is calculated from optimized linear combination of ΔGele, ΔGvdW, ΔGsolv, and SASA from regression

The regression model developed basing on linear response scheme is statistically ($r^2_{cv} = 0.802$, r^2=0.815, F=141.99) best fitted and consequently used for prediction of antimalarial activities (log RA) of the artemisinin analogues as reported in Table 16. The average root mean square error between predicted and experimental RA values was 0.291 obtained by leave-one-out cross validation technique further revealed the reliability of the model for prediction of antimalarial activity. However, we may observe that model using linear response scheme is better for predicting antimalarial activity than model using Glide score and ΔG_{bind} as descriptors.

Conclusions

We have presented herein an FEB calculation on the binding affinity of 150 artemisinin derivatives with PfATP6. The binding structures of these ligands in PfATP6 were predicted by flexible docking simulations. The docking result demonstrated that the docking simulation could satisfactorily reproduce a binding structure from a crystal structure of a SERCA/TG complex. Superposition of the binding structure of a whole set of ligands from docking simulations shows that these structurally similar ligands bind in a very similar pattern in PfATP6. They all bind at the same orientations which have been found in crystal structures of SERCA/TG. They bind in a similar position inside the PfATP6 active site and try to fit the binding pocket well. The calculated FEB for these ligands reasonably predicted the activity of this set of ligands. The calculated activity has good correlation to the experimental activity. The result shows that the linear combination of four energy terms: vdW, electrostatic, solvation (electrostatic part) and nonpolar energies optimized by regression has the power to express the binding affinity of a large set of ligands in the receptor. The Dock-MM-GBSA and eMBrAcE demonstrate a good ability on the binding structure prediction and binding energy determination to produce reasonable energies. The GBSA method predicted a

Table 17 Regression properties of energy parameters with experimental activities (Log RA)

	SASA	ΔG_{vdW}	ΔG_{ele}	ΔG_{solv}
Correlation factor with log RA	0.018	0.587	0.009	0.001
Intercept (B)	−0.492	−3.24	0.087	0.099
SE of B	0.34	0.241	0.081	0.088

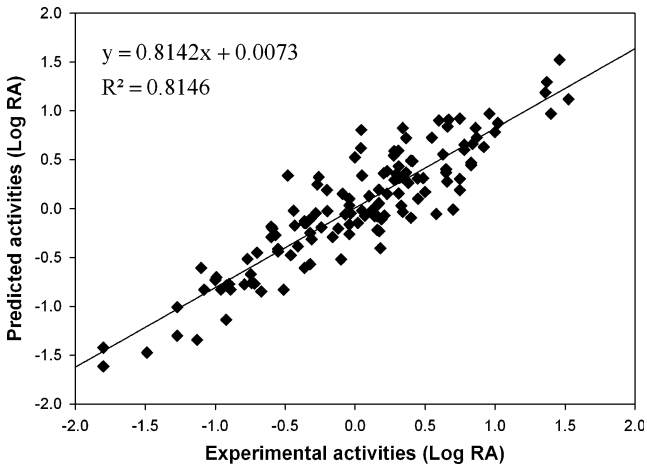

Fig. 9 Models for predicting antimalarial activity (Log RA) of the artemisinin derivatives based on free energy of binding (FEB)

reasonable solvation energy terms to enable a satisfactory FEB expression. In this work it is noticed that among these energy terms the ΔG_{vdW} has the most significant correlation to the activity (log RA). The binding modes of artemisinin and its derivatives showed hydrophobic interaction with PfATP6. In this work, GB and SASA methods were used to estimate the electrostatic and the nonpolar parts of solvation and produced satisfactory results in terms of good correlation to experimental activity.

References

1. Klayman DL (1985) Qinghaosu (artemisinin) an antimalarial drug from China. Science 228:1049–1055
2. Arrow KJ, Panosian CB, Geltband H (2004) Saving lives, buying time economics of malaria drugs in an age of resistance. National Academic, Washington, DC
3. Jefford CW (2001) Why artemisinin and certain synthetic peroxides are potent antimalarials. Implications for the mode of action. Curr Med Chem 8:1803–1826
4. Pandey AV, Tekwani BL, Singh RL, Chauhan VS (1999) Artemisinin, an endoperoxide antimalarial, disrupts the hemoglobin catabolism and hemin detoxification systems in malarial parasite. J Biol Chem 274:19383–19388
5. Haynes RK et al (2003) Artemisinin antimalarials do not inhibit hemozoin formation. Antimicrob Agents Chemother 47:1175
6. O'Neill P et al (2000) Biomimetic Fe(II)-mediated degradation of arteflene (Ro-42–1611). The first EPR spin-trapping evidence for the previously postulated secondary carbon-centered cyclohexyl radical. J Org Chem 65:1578–1582
7. Hawley SR et al (1998) Relationship between antimalarial drug activity, accumulation, and inhibition of heme polymerization in Plasmodium falciparum in vitro. Antimicrob Agents Chemother 42:682–686
8. Ellis DS et al (1985) The chemotherapy of rodent malaria, XXXIX. Ultrastructural changes following treatment with artemisinine of Plasmodium berghei infection in mice, with observations of the localization of [3H]-dihydroartemisinine in P. falciparum in vitro. Ann Trop Med Parasitol 79:367–374
9. ter Kuile F, White NJ, Holloway PH, Pasvol G, Krishna S (1993) Plasmodium falciparum: in vitro studies of the pharmacodynamic properties of drugs used for the treatment of severe malaria. Exp Parasitol 76:85–95
10. Eckstein-Ludwig U, Webb RJ, van Goethem IDA, East JM, Lee AG, Kimura M, O'Neill PM, Bray PG, Ward SA, Krishna S (2003) Artemisinins target the SERCA of Plasmodium falciparum. Nature 424:957–961
11. Kuhlbrandt W (2004) Biology, structure and mechanism of P-type ATPases. Nat Rev Mol Cell Biol 5:282–295
12. Toyoshima C, Nakasako M, Nomura H, Ogawa H (2000) Crystal structure of the calcium pump of sarcoplasmic reticulum at 2.6 angstrom resolution. Nature 405:647–655
13. Toyoshima C, Nomura H (2002) Structural changes in the calcium pump accompanying the dissociation of calcium. Nature 418:605–611
14. Toyoshima C, Mizutani T (2004) Crystal structure of the calcium pump with a bound ATP analogue. Nature 430:529–535
15. Sorensen TLM, Moller JV, Nissen P (2004) Phosphoryl transfer and calcium ion occlusion in the calcium pump. Science 304:1672–1675
16. Gardner MJ, Hall N, Fung E, White O, Berriman M, Hyman RW, Carlton JM, Pain A, Nelson KE, Bowman S, Paulsen IT, James K, Eisen JA, Rutherford K, Salzberg SL, Craig A, Kyes S, Chan MS, Nene V, Shallom SJ, Suh B, Peterson J, Angiuoli S, Pertea M, Allen J, Selengut J, Haft D, Mather MW, Vaidya AB, Martin DM, Fairlamb AH, Fraunholz MJ, Roos DS, Ralph SA, McFadden GI, Cummings LM, Subramanian GM, Mungall C, Venter JC, Carucci DJ, Hoffman SL, Newbold C, Davis RW, Fraser CM, Barrell B (2002) Genome sequence of the human malaria parasite Plasmodium falciparum. Nature 419:498–511
17. Prime version 1.5, Macromodel version 9.1, Schrodinger, LLC, New York, NY, 2005
18. Laskowski RA, MacArthur MW, Moss DS, Thornton JM (1993) *PROCHECK*: a program to check the stereochemical quality of protein structures. J Appl Crystallogr 26:283–291
19. Ramachandran GN, Ramakrishnan C, Sasisekharan V (1963) Stereochemistry of polypeptide chain configurations. J Mol Biol 7:95–99
20. Eisenberg D, Luthy R, Bowie JU (1997) VERIFY3D: assessment of protein models with three-dimensional profiles. Methods Enzymol 277:396–404
21. Uhlemann AC, Cameron A, Eckstein-Ludwig U, Fischbarg J, Iserovich P, Zuniga FA, East M, Lee A, Brady L, Haynes RK, Krishna S (2005) Nat Struct Mol Biol 12:628–629
22. Woolfrey JR, Avery MA, Doweyko AM (1998) Comparison of 3D quantitative structure-activity relationship methods: analysis of the in vitro antimalarial activity of 154 artemisinin analogues by hypothetical active-site lattice and comparative molecular field analysis. J Comput-Aided Mol Des 12(2):165–181
23. Acton N, Karle JM, Miller RE (1993) Synthesis and antimalarial activity of some 9-substituted artemisinin derivatives. J Med Chem 36:2552–2557
24. Lin AJ, Margaret L, Klayman DL (1989) Antimalarial activity of new water-soluble dihydroartemisinin derivatives. 2. Stereospecificity of the ether side chain. J Med Chem 32:1249–1252
25. Posner GH, Oh CH, Gerena L, Milhous WK (1992) Extraordinarily potent antimalarial compounds: new, structurally simple, easily synthesized, tricyclic 1, 2, 4-trioxanes. J Med Chem 35:2459–2467
26. Avery MA, Bonk JD, Chong WKM, Mehrotra S, Miller R (1995) Structure-activity relationships of the antimalarial agent artemisinin. 2. Effect of heteroatom substitution at O-11: synthesis and bioassay of N-Alkyl-11-aza-9-desmethylartemisinins. J Med Chem 38:5038–5044
27. Avery MA, Mehrotra S, Bonk JD, Vroman JA, Goins DK (1996) Structure-activity relationships of the antimalarial agent artemisinin 4. Effect of substitution at C-3. J Med Chem 39:2900–2906
28. Pinheiro JC, Ferreira MMC, Romero OAS (2001) Antimalarial activity of dihydroartemisinin derivatives against *P. falciparum* resistant to mefloquine: a quantum chemical and multivariate study. J Mol Struct THEOCHEM 572:35–44
29. Leban I, Golic L, Japelj M (1988) Crystal and molecular structure of qinghaosu: a redetermination. Acta Pharm Jugosl 38:71–77
30. Lisgarten JN, Potter BS, Bantuzeko C, Palmer RA (1998) Structure, absolute configuration, and conformation of the antimalarial compound, artemisinin. J Chem Crystallogr 28:539–543
31. Bernardinelli G, Jefford CW, Maric D, Thomson C, Weber J (1994) Computational studies of the structures and properties of potential anti-malarial compounds based on the 1, 2, 4-trioxane ring structure: I artemisinin-like molecules. Int J Quant Chem: Quant Biol Symp 21:117–131
32. Posner GH, Cumming JN, Ploypradith P, Oh CH (1995) Evidence for Fe(iv) O in the molecular mechanismof action of the trioxane antimalarial artemisinin. J Am Chem Soc 117:5885–5886
33. Haynes RK, Vonwiller SC (1996) The behaviour of qinghaosu (artemisinin) in the presence of hemin iron (II) and (III). Tetrahedron Lett 37:253–256
34. Rafiee MA, Hadipour NL, Naderi-manesh H (2005) The role of charge distribution on the antimalarial activity of artemisinin analogs. J Chem Inf Model 45:366–370

35. Friesner RA, Banks JL, Murphy RB, Halgren TA, Klicic JJ, Mainz DT, Repasky MP, Knoll EH, Shelley M, Perry JK, Shaw DE, Francis P, Shenkin PS (2004) Glide: a new approach for rapid, accurate docking and scoring 1 method and assessment of docking accuracy. J Med Chem 47:1739–1749
36. Eldridge MD, Murray CW, Auton TR, Paolini GV, Mee RP (1997) Empirical scoring functions: the development of a fast empirical scoring function to estimate the binding affinity of ligands in receptor complexes. J Comput-Aided Mol Des 11:425–445
37. Guvench O, Weiser J, Shenkin PS, Kolossváry I, Still WC (2002) Application of the frozen atom approximation to the GB/SA continuum model for solvation free energy. J Comput Chem 23:214–221
38. Wu X, Milne JLS, Borgnia MJ, Rostapshov AV, Subramaniam S, Brooks BR (2003) A core-weighted fitting method for docking atomic structures into low-resolution maps: application to cryo-electron microscopy. J Struct Biol 141:63–76
39. Todorov NP, Mancera RL, Monthoux PH (2003) A new quantum stochastic tunnelling optimisation method for protein-ligand docking. Chem Phys Lett 369:257–263
40. Reynolds CH (1995) Estimating liphophilicity using GB/SA continuum solvation Model: a direct method for computing partition coefficients. J Chem Inf Comput Sci 35:738–742
41. Haynes RK, Krishna S (2004) Artemisinins: activities and actions. Microbes Infect 6:1339–1346